Acta Crystallographica Section D
Biological Crystallography
ISSN 1399-0047

The rotational order–disorder structure of the reversibly photoswitchable red fluorescent protein rsTagRFP

Sergei Pletnev,[a,b]* Fedor V. Subach,[c] Vladislav V. Verkhusha[c] and Zbigniew Dauter[b]*

[a]Leidos Biomedical Research Inc., Basic Research Program, Argonne National Laboratory, Argonne, IL 60439, USA, [b] Macromolecular Crystallography Laboratory, National Cancer Institute, Argonne National Laboratory, Argonne, IL 60439, USA, and [c]Department of Anatomy and Structural Biology, Albert Einstein College of Medicine, Bronx, NY 10461, USA

Correspondence e-mail: pletnevs@mail.nih.gov, dauter@anl.gov

Received 3 June 2013
Accepted 3 September 2013

PDB Reference: rsTagRFP, 4kpi

The rotational order–disorder (OD) structure of the reversibly photoswitchable fluorescent protein rsTagRFP is discussed in detail. The structure is composed of tetramers of 222 symmetry incorporated into the lattice in two different orientations rotated 90° with respect to each other around the crystal *c* axis and with tetramer axes coinciding with the crystallographic twofold axes. The random distribution of alternatively oriented tetramers in the crystal creates the rotational OD structure with statistically averaged *I*422 symmetry. Despite order–disorder pathology, the structure of rsTagRFP has electron-density maps of good quality for both non-overlapping and overlapping parts of the model. The crystal contacts, crystal internal architecture and a possible mechanism of rotational OD crystal formation are discussed.

1. Introduction

Since the early days of crystallography, researchers have faced crystals in which the molecules are arranged stochastically. These crystals could be recognized by their unusual diffraction patterns, with some classes of reflections having modulated intensities and diffuse profiles. To describe such cases, Dornberger-Schiff developed the order–disorder theory and introduced the first classification of OD structures consisting of three types: A, B and C (Dornberger-Schiff, 1956). Since this early work, OD theory has significantly developed and is nowadays used for the explanation of polytypism, twinning and lattice-translocation defects, presenting a powerful tool for the description and modeling of OD structures (Ferraris *et al.*, 2004). OD theory has successfully been applied to all major classes of chemical compounds from inorganic materials to proteins. In the field of minerals and inorganic synthetic compounds, OD theory has successfully been used to describe nonstandard structural arrangements (Ferraris *et al.*, 2004). In the field of low-molecular-weight organic compounds, it has been used to describe numerous atypical structures; to name a few, urotropin azelate (Bonin *et al.*, 2003), tris-(bicyclo [2.1.1]hexeno)benzene (Birkedal *et al.*, 2003; Ferraris *et al.*, 2004) and nonactin (Dornberger-Schiff, 1966). In the field of protein crystallography, OD theory has helped to classify and solve structures with twinning and lattice-translocation defects, including antibody 17/9 (Schulze-Gahmen *et al.*, 1993), an RNA dodecamer (Lietzke *et al.*, 1996), a Lon domain (Dauter *et al.*, 2005), a Fab–peptide complex (Dhillon *et al.*, 2008), HslU chaperone (Trame & McKay, 2001), φ29 DNA polymerase (Wang *et al.*, 2005), bacterial L-2-haloacid dehalogenase (Rye *et al.*, 2007), a SARS S1–antibody complex (Hwang *et al.*, 2006), H1N1 neuraminidase (Zhu *et al.*, 2008), bacterial carboxysome shell (Tanaka *et al.*, 2008) and others.

During study of the reversibly photoswitchable fluorescent protein rsTagRFP (Subach *et al.*, 2010) we obtained two varieties of crystals: prisms and rods. The prismatic crystals diffracted to 1.78 Å resolution, belonged to space group *P*1 and had a conventional diffraction pattern. The structure of rsTagRFP obtained from this crystal form has been described in detail in Pletnev *et al.* (2012). The rods diffracted to 1.58 Å resolution and had an abnormal diffraction pattern in which lines of well shaped reflection profiles alternated with diffuse streaks (Fig. 1). This diffraction pattern is similar to that observed previously for the fluorescent protein FP480 and ascribed to rotational order–disorder pathology (Pletnev *et al.*, 2009).

In our earlier paper on the rotational OD structure of FP480 (Pletnev *et al.*, 2009) we outlined the internal architecture of the crystal, addressing the question of how the packing of the rotational OD crystal is organized. Here, we address the next logical question of why such unusual packing is possible.

2. Materials and methods

2.1. Protein expression and purification

To express protein for crystallization, a fragment encoding rsTagRFP with an N-terminal His tag was cloned into pQE30 vector (Qiagen, Valencia, USA) and transformed into *Escherichia coli* strain XL1 Blue (Invitrogen, Carlsbad, USA). The bacterial culture was incubated overnight at 310 K. No IPTG induction was necessary since promoter leakage was sufficient for effective expression. To achieve complete protein maturation the culture was additionally incubated at 298 K for 12 h. Cells were pelleted by centrifugation, resuspended in phosphate-buffered saline and lysed by sonication. The protein was purified by immobilized metal-affinity chromatography using TALON resin (Clontech Laboratories, Mountain View, USA) followed by size-exclusion chromatography using a Superdex 200 (16/60) column (GE Healthcare, Piscataway, USA).

2.2. Crystallization

For crystallization, the protein was transferred into a buffer consisting of 10 m*M* Tris–HCl pH 8.0 and was concentrated to 30 mg ml^{-1}. Buffer exchange and protein concentration was performed in VivaSpin 6 10 kDa MWCO sample concentrators (Vivascience, Littleton, USA). An initial search for crystallization conditions was carried out using a Mosquito Robotic Crystallization System (TTP LabTech, Royston, England) and yielded several successful hits. The crystallization was scaled up by the hanging-drop vapour-diffusion method. The rotational order–disorder crystals of rsTagRFP were obtained from 2 µl protein solution mixed with 2 µl well solution (0.2 *M* ammonium nitrate, 20% PEG 3350) incubated against 500 µl of the same reservoir at 293 K. The crystals achieved their final size in two weeks.

2.3. Data collection and processing

X-ray diffraction data were collected on the SER-CAT 22-BM beamline at the Advanced Photon Source (Argonne National Laboratory, Argonne, USA). Diffraction intensities were registered on a MAR225 CCD detector (Rayonix, Evanston, USA). Prior to data acquisition, the crystals were incubated in a cryoprotecting solution consisting of 20% glycerol and 80% well solution for 10–20 s and were flash-cooled in a 100 K nitrogen stream. Cryogenic temperature was maintained using a CryoJetXL cooling device (Oxford Cryosystems, Oxford, England). 120° of data collected with an oscillation angle of 0.5° at an X-ray beam wavelength of 1 Å comprised a complete data set. Diffraction images were

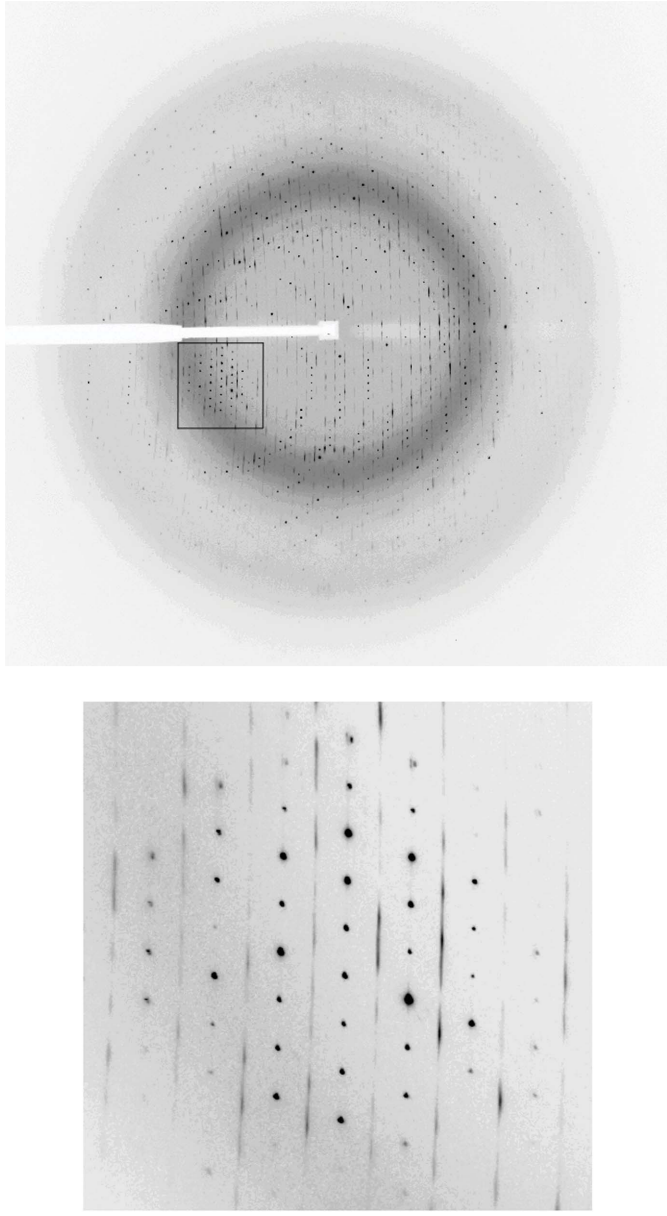

Figure 1
The diffraction pattern obtained from a rotational order–disorder crystal of rsTagRFP. The enlarged section of the frame shows the lines of diffuse reflections alternating with well shaped diffraction spots.

Table 1
Diffraction data and refinement statistics for the rotational OD crystal structure of rsTagRFP (PDB entry 4kpi).

Values in parentheses are for the last resolution shell.

Data statistics	
Space group	*I*422
Molecules per asymmetric unit	0.5
Unit-cell parameters (Å)	a = 92.7, c = 53.1
Resolution (Å)	30.0–1.58 (1.64–1.58)
Total reflections	104157
Unique reflections	15284
Completeness (%)	94.4 (62.2)
$\langle I/\sigma(I)\rangle$	36.3 (2.2)
$R_{\rm merge}$	0.046 (0.596)
Multiplicity	6.8 (4.1)
Refinement statistics	
No. of reflections	14283
$R_{\rm work}/R_{\rm free}$	0.225/0.279
Geometry statistics (r.m.s.d.)	
Bonds (Å)	0.014
Angles (°)	1.79
Chirality (Å^3)	0.083
Planarity (Å)	0.008
Dihedrals (°)	15.9
Ramachandran statistics (%)	
Favored	96.8
Allowed	2.3
Outliers	0.9

indexed, integrated and scaled with *HKL*-2000 (Otwinowski & Minor, 1997). Corresponding data-processing statistics are given in Table 1.

2.4. Structure solution and refinement

The X-ray diffraction data were tested for twinning and translation disorders with *XPREP* (Sheldrick, 2000), *TRUNCATE* (Winn *et al.*, 2011) and the UCLA MBI Twin Detection server (http://services.mbi.ucla.edu/Twinning/; Padilla & Yeates, 2003). The rotational OD structure of rsTagRFP was solved by the molecular-replacement method with *MOLREP* (Vagin & Teplyakov, 2010) using the structure of a single monomer of rsTagRFP obtained in a conventional crystal form (PDB entry 3u8a; Pletnev *et al.*, 2012) as the search model. Owing to an inevitable overlap between symmetry-related molecules in the rotational OD structure, the search for the molecular-replacement solution was carried out with a disabled packing function. Structure refinement was performed with *REFMAC* (Murshudov *et al.*, 2011), *Coot* (Emsley & Cowtan, 2004) and finally with *phenix.refine* (Adams *et al.*, 2010). The specific details of the refinement are listed below. In *REFMAC*, to disable repulsions between overlapping atoms that are activated when the sum of the occupancies of symmetry-related atoms in the structure is equal to unity, the occupancy of each individual atom of the model was set to 0.49. Alternatively, the instruction 'vdwrestraints exclude between chains A' can be used. In *phenix.refine*, to preserve the occupancies of individual atoms of the model and to disable penalties for close contacts between the model (chain *A*) and overlapping chains, the instructions 'occupancies.remove_selection=chain A' and 'pdb_interpretation.custom_nonbonded_symmetry_exclusions=chain A' were incorporated in the refinement protocol. An example of the command script is given in the Supporting Information.[1] In *Coot*, real-space refinement was avoided for the truly overlapped parts of the structure, as the program is unable to properly fit atoms of the model into overlapped peaks in electron-density maps. Ordered solvent molecules were added to the appropriate electron-density peaks using *Coot* and *phenix.refine*. Structure validation was performed with *Coot* and *PROCHECK* (Laskowski *et al.*, 1996). The corresponding refinement statistics are given in Table 1.

Table 2
Intensity statistics for the rotational order–disorder rsTagRFP data.

Wilson ratios	Observed	Theoretical, untwinned	Theoretical, 50% twinned
$\langle I^2\rangle/\langle I\rangle^2$, acentric	1.969	2.0	1.5
$\langle I^2\rangle/\langle I\rangle^2$, centric	3.188	3.0	2.0
L-tests†			
$\langle\|L\|\rangle$	0.490	0.5	0.375
$\langle L^2\rangle$	0.323	0.333	0.2

† According to Padilla & Yeates (2003).

3. Results and discussion

3.1. Validation of the rotational OD pathology of rsTagRFP crystals

The diffraction patterns obtained from the rod-shaped crystals of rsTagRFP contained low-intensity diffuse reflections between the principal, well defined Bragg reflections (Fig. 1). These additional reflections were located in the a^*b^* layers between the well shaped reflections and their streaks were elongated in the a^*b^* plane. The presence of diffuse streaks on every image of the data set suggests that the three-dimensional reciprocal lattice consists of alternating well defined and diffuse a^*b^* planes. The diffuse reflections could not be processed and thus were excluded from the final data set. The well shaped Bragg reflections could be satisfactorily merged in space group *I*422 with an $R_{\rm merge}$ of 0.046 (Table 1). In spite of the excellent data statistics, the Matthews coefficient calculated for the given unit-cell parameters and the molecular weight of a single molecule of rsTagRFP (27 619 Da) was found to be 1.0 Å^3 Da^{-1}, which would only allow one half of a monomer per asymmetric unit.

The observed abnormal diffraction pattern and the unrealistic value of the Matthews coefficient could correspond to typical pathologies known for protein crystals: twinning and/or translational order–disorder (alternatively termed lattice-translocation defects). The presence of merohedral twinning, which is theoretically possible for tetragonal symmetry, can typically be verified by Wilson ratios and other intensity statistics (Padilla & Yeates, 2003), whereas cases of translational order–disorder manifest themselves as the presence of significant off-origin peaks in the native Patterson map. The intensity statistics (Table 2) calculated for the rsTagRFP data showed no characteristics typical of merohe-

[1] Supporting nformation has been deposited in the IUCr electronic archive (Reference: YT5058).

dral twinning, with Wilson ratios $\langle I^2\rangle/\langle I\rangle^2$ of 3.188 and 1.969 for centric and acentric reflections, respectively, a nearly perfect shape of the $N(|z|)$ and $N(|L|)$ plots (Fig. 2) and an L ratio of 0.49 (Padilla & Yeates, 2003). The nearly perfect agreement of the reflections classified as centric with the theoretical curve of the $N(|z|)$ plot confirms the correct choice of $I422$ symmetry. The native Patterson map of rsTagRFP has the highest off-origin peaks at a level of 6% of the origin peak, indicating the absence of translational pseudosymmetry. Similar validation results were obtained for the rotational OD structure of FP480 (Pletnev *et al.*, 2009), which has a diffraction pattern that closely resembles that of rsTagRFP. Thus, it is most likely that the pathological crystals of FP480 and rsTagRFP have the same type of disorder.

The structure of rsTagRFP was solved by the molecular-replacement method. The molecular-replacement solution of rsTagRFP corresponds to a monomer. The twofold symmetry elements of space group $I422$ complete the monomer of rsTagRFP to a tetramer that occupies a special position with its center coinciding with the origin of the unit cell and its twofold axes coinciding with the diagonal crystallographic twofold axes of space group $I422$. The fourfold symmetry axis of $I422$ generates the second tetramer, which is located in the same place and rotated 90° with respect to the first tetramer (Fig. 3). Despite the order–disorder pathology, the structure of rsTagRFP has electron-density maps of very good quality for

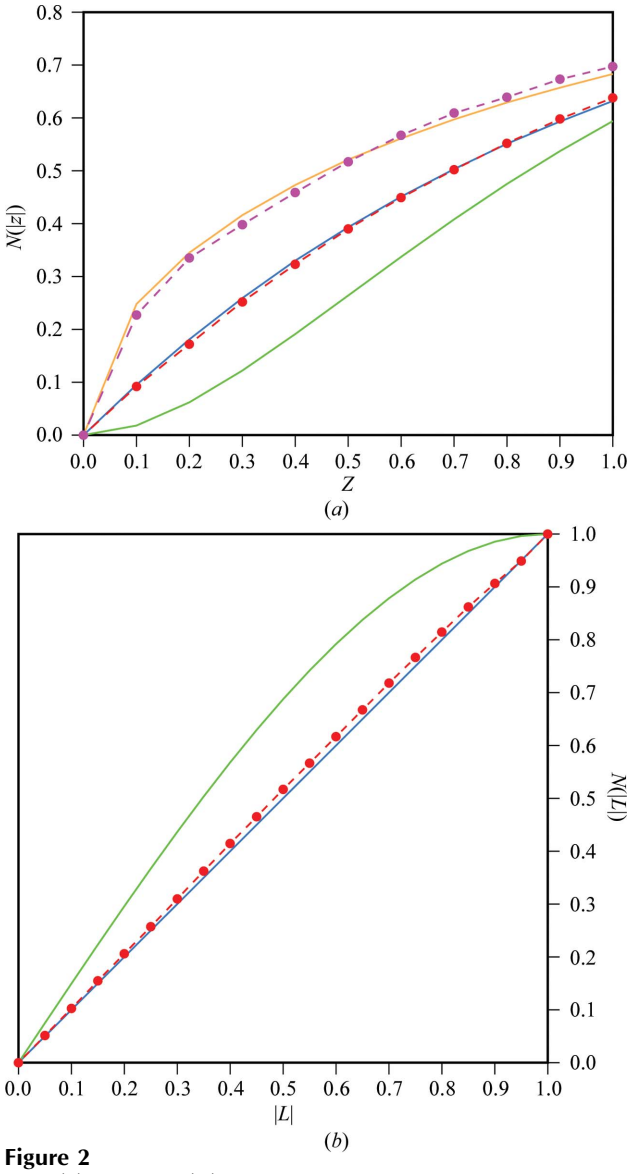

Figure 2
(*a*) $N(|z|)$ and (*b*) $N(|L|)$ plots calculated for the rotational order–disorder rsTagRFP crystal. In both plots solid green lines correspond to the theoretical perfectly twinned case. The solid orange and blue lines in the $N(|z|)$ plot correspond to theoretical untwinned cases calculated for centric and acentric reflections, respectively. The solid blue line in the $N(|L|)$ plot corresponds to the theoretical untwinned case calculated for all reflections. In both plots dashed lines and dots represent the experimental statistics calculated from the measured data.

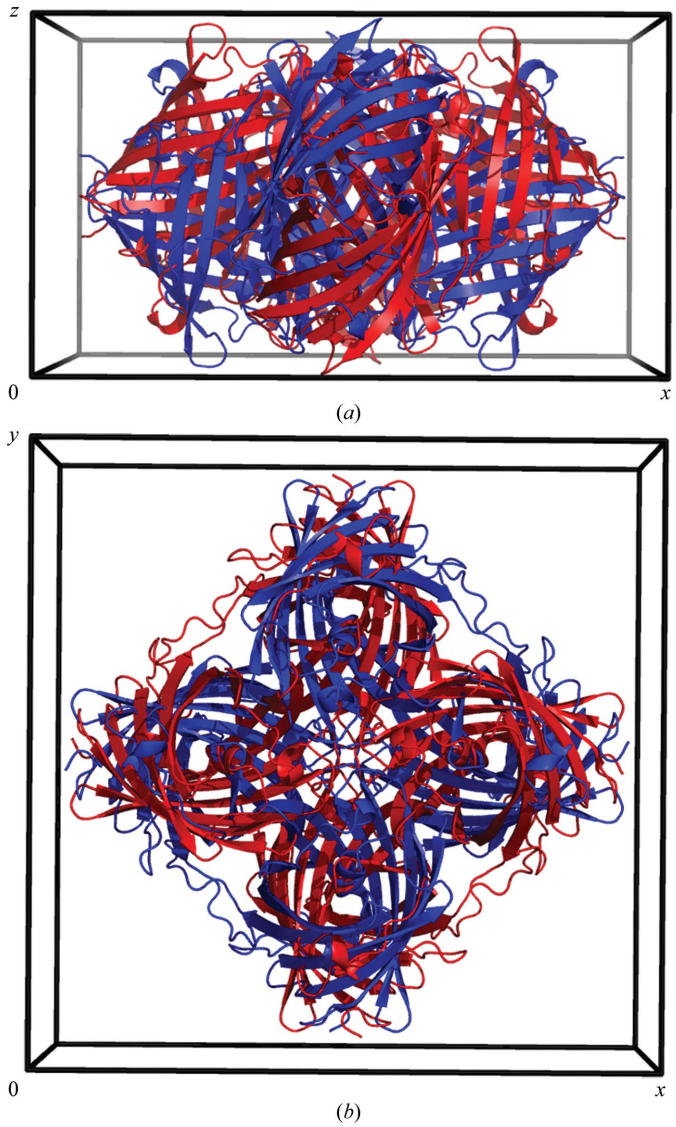

Figure 3
Rotational OD structure of rsTagRFP in the statistically averaged space group $I422$. Two tetramers of 222 symmetry, blue and red, overlapping at 90° with respect to each other occupy the 422 special position in the unit cell. Their centers coincide with the origin or the center of the unit cell and their 222 axes coincide with the z and diagonal axes of the cell. (*a*) The view along the crystallographic y axis. (*b*) The view along the crystallographic z axis.

both the non-overlapping and the overlapping parts of the structure (Fig. 4).

3.2. The mechanism of crystal growth of rotational OD crystals of rsTagRFP

Protein crystals are held together by the same forces that stabilize macromolecular assemblies such as protein–protein complexes and oligomeric proteins. However, in crystals, the nonspecific interfaces between the protein molecules are much smaller than the biologically relevant interfaces in complexes and oligomeric proteins. Therefore, during the course of crystallization, for proteins with complementary surfaces it is thermodynamically more favorable to first form oligomers and then to crystallize. Nearly two decades ago, Janin and Rodier analyzed 1320 pairwise interfaces of protein crystals and found that the average crystal contact covers an area of 570 Å^2 and has one hydrogen bond per 280 Å^2 of buried surface (Janin & Rodier, 1995). However, some interfaces involve a single amino-acid residue on each partner molecule and bury 50 Å^2, whereas others involve 100 residues and bury over 2000 Å^2 (Janin & Rodier, 1995). The analysis of biologically relevant interfaces demonstrated that a typical interface in a protein–protein complex covers about 1500 Å^2 and contains about ten hydrogen bonds, *i.e.* one hydrogen bond per 150 Å^2 of buried area (Janin, 1995), whereas the contacts between subunits in oligomeric proteins have the most extensive interfaces, covering 3000–10 000 Å^2 of surface with an average hydrogen-bond density of one hydrogen bond per 200 Å^2 of buried surface (Janin *et al.*, 1988). Thus, the

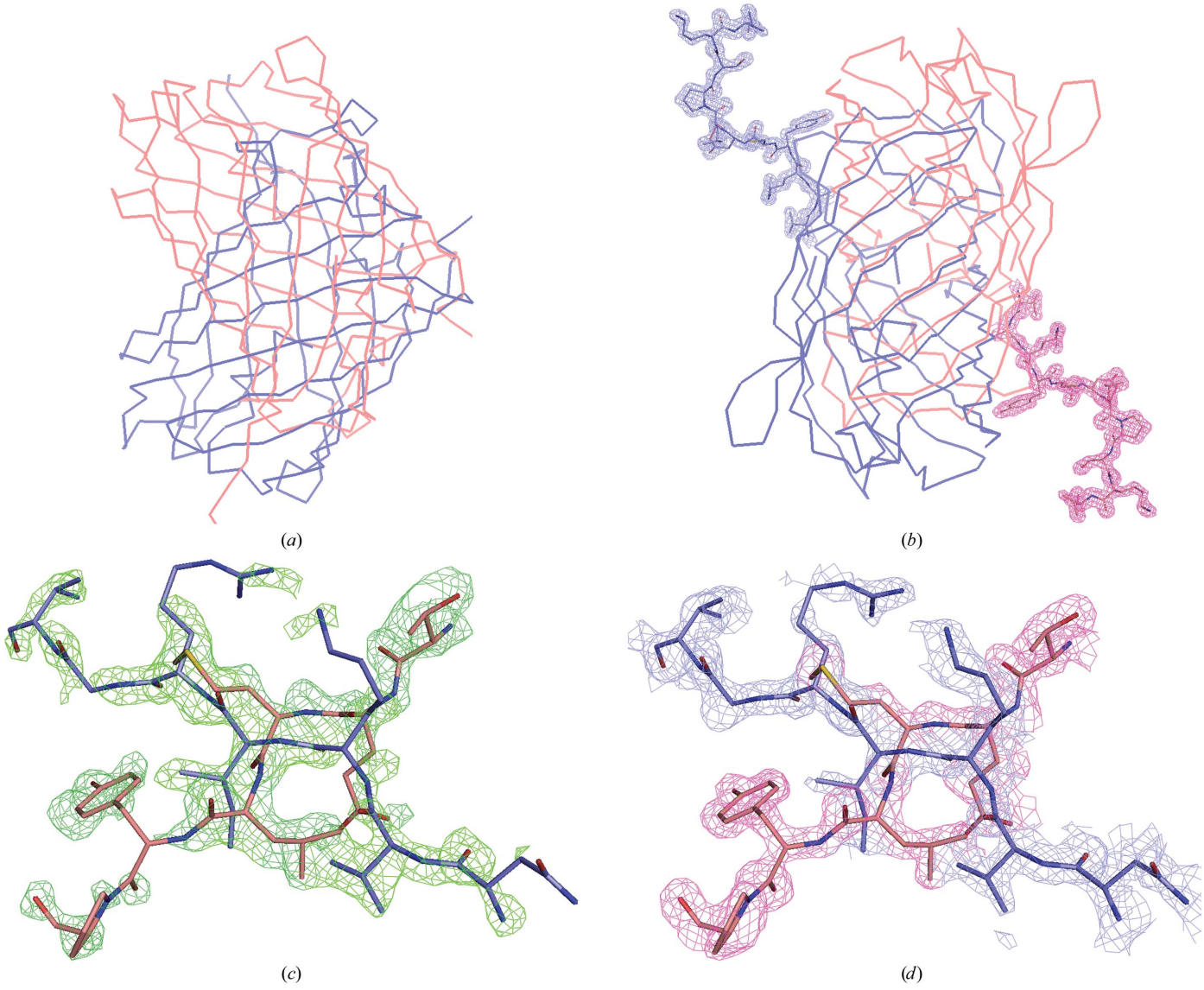

Figure 4
(*a*) A view of overlapped monomers of rsTagRFP. Blue and pink molecules are related by the crystallographic twofold axis. (*b*) A 90° rotated view of the same monomers. Non-overlapping parts of the structure, residues 222–232 (VARYCDLPSKL), are shown as a $2F_o - F_c$ electron-density map contoured at the 1.0σ level. The color of the $2F_o - F_c$ density matches the color of the chains for clarity. (*c*) Composite OMIT map, contoured at the 2.5σ level, calculated for structures lacking residues 118–124 (NVKLRGV; blue) and 144–149 (TEMLYP; pink). (*d*) The $2F_o - F_c$ electron-density map, contoured at the 1.0σ level, calculated for the same fragment of the structure.

Table 3
Buried surface area (BSA) between symmetry-related tetramers of rsTagRFP in the crystal.

Tetramer 1 orientation/ symmetry	Tetramer 2 orientation/ symmetry	BSA† (Å^2)	No. of hydrogen bonds
0° x, y, z	0° $x+1, y, z$	67	0
0° x, y, z	90° $x+1, y, z$	52	0
0° x, y, z	0° $x+1/2, y+1/2, z+1/2$	614	2
0° x, y, z	90° $x+1/2, y+1/2, z+1/2$	284	1
90° x, y, z	90° $x+1/2, y+1/2, z+1/2$	99	0
0° x, y, z	0° $x, y, z+1$	950	0
0° x, y, z	90° $x, y, z+1$	1737	16

average crystal-packing interface constitutes only one third of that of a complex and one sixth of that of a homodimer. Nevertheless, crystal packing buries much of the protein surface because in an average crystal each molecule has 8–10 neighbors (Janin *et al.*, 2008).

What sequence of events is likely to occur in the crystallization drop during crystallization of rsTagRFP? At concentrations below 10 mg ml^{-1} rsTagRFP exists as a monomer in solution (Subach *et al.*, 2010). When its concentration increases beyond this point, the monomers start to assemble into dimers and then tetramers. When these tetramers reach a supersaturated state, they start to associate, forming crystals. To elucidate the ability of the rsTagRFP tetramers to integrate into the growing crystal in two different orientations, we analyzed all possible combinations of the adjacent tetramers and the interfaces between them (Table 3).

The Voronoi polyhedron of the point located at the center of the *I*-type cell is a cuboctahedron. Indeed, the shape of the two rsTagRFP tetramers overlapped at 90° can be approximated by a distorted (flattened) cuboctahedron, as illustrated in Fig. 5. Such a polyhedron has tetragonal symmetry and possesses three kinds of faces: two squares perpendicular to the fourfold axis, four smaller rhombuses across the crystallographic twofold axes and eight distorted hexagons across the space diagonals of the unit cell. In analogy to the three types of pseudo-cuboctahedral faces, the contacts between adjacent tetramers in the crystal can be divided into three groups: contacts along the x and y crystal axes, contacts along space diagonals of the unit cell and contacts along the z axis of the crystal. (i) The buried surface areas between (0° x, y, z–0° $x+1, y, z$) and (0° x, y, z–90° $x+1, y, z$) tetramers are modest: 67 and 52 Å^2 for the 0°–0° and 0°–90° assemblies, respectively (Table 3). (ii) The contacts along space diagonals are more extensive: the corresponding buried surface areas are 614, 284 and 99 Å^2 for (0° x, y, z–0° $x+1/2, y+1/2, z+1/2$), (0° x, y, z–90° $x+1/2, y+1/2, z+1/2$) and (90° x, y, z–90° $x+1/2, y+1/2, z+1/2$) interfaces, respectively. (iii) The contacts along the z direction are the most extensive: interfaces between (0° x, y, z–0° $x, y, z+1$) and (0° x, y, z–90° $x, y, z+1$) pairs of tetramers bury 950 and 1737 Å^2, respectively, which puts them in line with the biologically relevant interfaces of protein–protein complexes.

Owing to the 222 symmetry, with the exception of the (0° x, y, z–90° $x+1/2, y+1/2, z+1/2$) pair, the contacts between the adjacent tetramers of rsTagRFP are formed by the same groups of residues (Table 4). Contacting residues are located mostly in the loop areas of the β-barrel. The most significant interfaces are formed by (0° x, y, z–0° $x, y, z+1$), (0° x, y, z–90° $x, y, z+1$) and (0° x, y, z–0° $x+1/2, y+1/2, z+1/2$) pairs. The tetramers in the pairs (0° x, y, z–0° $x+1, y, z$) and (0° x, y, z–90° $x+1/2, y+1/2, z+1/2$) form single-amino-acid contacts, whereas the pairs (0° x, y, z–90° $x+1, y, z$) and (90° x, y, z–90° $x+1/2, y+1/2, z+1/2$) interact with each other only *via* water molecules. A complete list of contacts between adjacent tetramers is presented in Supplementary Table S1.

The scenario of crystal growth along the x and y axes is unlikely since the buried surface areas between tetramers in the x and y directions are much smaller than those between tetramers along space diagonals and the z direction. Although it is clear that a certain percentage of tetramers join the crystal along its space diagonals, the buried surface areas along them are likely to be too modest to make it a preferential direction of crystal growth. The buried surface areas between the tetramers connected vertically are the greatest, suggesting that the association of tetramers along the z direction is thermodynamically most favorable and occurs more often than association along the x, y or space-diagonal directions. This preferential direction of crystal growth is in good agreement with a rod crystal shape having the longest dimension coinciding with the crystal z axis.

The similarity of the contacts between the tetramers along the z direction to the interfaces of protein–protein complexes enables vertical association of the tetramers at concentrations below saturated. Therefore, one can propose a scenario of crystal growth in which individual tetramers first associate into pairs or even longer assemblies (stacks) in solution and the stacks are then incorporated in the crystal.

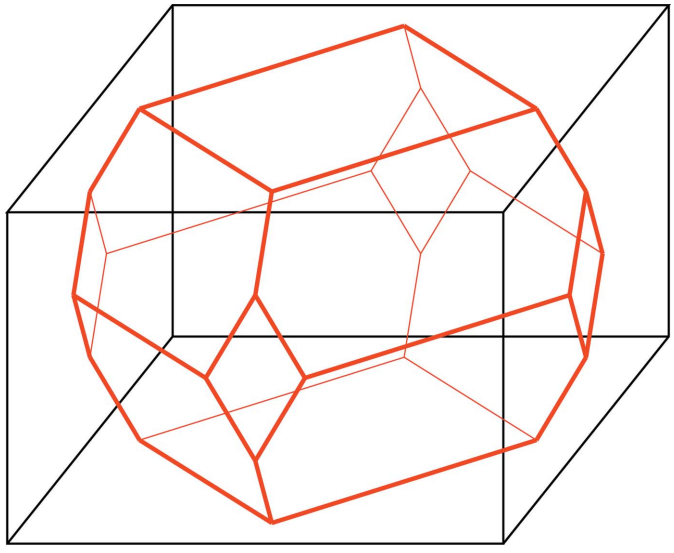

Figure 5
The Voronoi polyhedron of the point located at the center of the *I*-type cell. Such a polyhedron has tetragonal symmetry and possesses three kinds of faces: two squares perpendicular to the fourfold axis, four smaller rhombuses across the twofold axes and eight distorted hexagons across the space diagonals of the unit cell.

Vertical association of tetramers could occur in two different ways: non-alternating, when the stack is formed by similarly oriented tetramers (*i.e.* 0°–0°–0°–0–... or 90°–90°–90°–90°–...; Fig. 6*a*), and alternating, when the stack consists of alternatively oriented tetramers (*i.e.* 0°–90°–0°–90°–...; Fig. 6*b*). The buried surface area between 0° *x*, *y*, *z* and 90° *x*, *y*, *z* + 1 tetramers is almost two times larger than the buried surface area between 0° *x*, *y*, *z* and 0° *x*, *y*, *z* + 1 tetramers. Moreover, the interface between 0° *x*, *y*, *z* and 90° *x*, *y*, *z* + 1 tetramers contains 16 hydrogen bonds, whereas the interface between 0° *x*, *y*, *z* and 0° *x*, *y*, *z* + 1 tetramers does not have any hydrogen bonds at all. Thus, it is more likely that the stacks are formed with alternating 0° and 90° tetramers.

Table 4
The list of contacting residues between adjacent tetramers within a 4 Å cutoff distance.

Orientation		Contacting residues	
Tetramer 1	Tetramer 2	Tetramer 1	Tetramer 2
0° *x*, *y*, *z*	0° *x* + 1, *y*, *z*	Lys6	Lys6
0° *x*, *y*, *z*	90° *x* + 1, *y*, *z*	Glu7†	Glu7†
0° *x*, *y*, *z*	0° *x* + 1/2, *y* + 1/2, *z* + 1/2	Gly75, Pro225, Ser226, Lys227, Leu228	Gly75, Pro225, Ser226, Lys227, Leu228
0° *x*, *y*, *z*	90° *x* + 1/2, *y* + 1/2, *z* + 1/2	Gln74	Val46, Glu47
90° *x*, *y*, *z*	90° *x* + 1/2, *y* + 1/2, *z* + 1/2	Val46†	Va46†
0° *x*, *y*, *z*	0° *x*, *y*, *z* + 1	Lys136, Val165, Gly166, Lys185, Ala205, Asp206	Lys136, Val165, Gly166, Lys185, Ala205, Asp206
0° *x*, *y*, *z*	90° *x*, *y*, *z* + 1	Gln134, Lys136, Arg201, Lys203, Glu204, Ala205, Asp206, Lys207, Glu208	Gln134, Lys136, Arg201, Lys203, Glu204, Ala205, Asp206, Lys207, Glu208

† No direct contacts are formed; however, the tetramers contact with each other *via* water molecules.

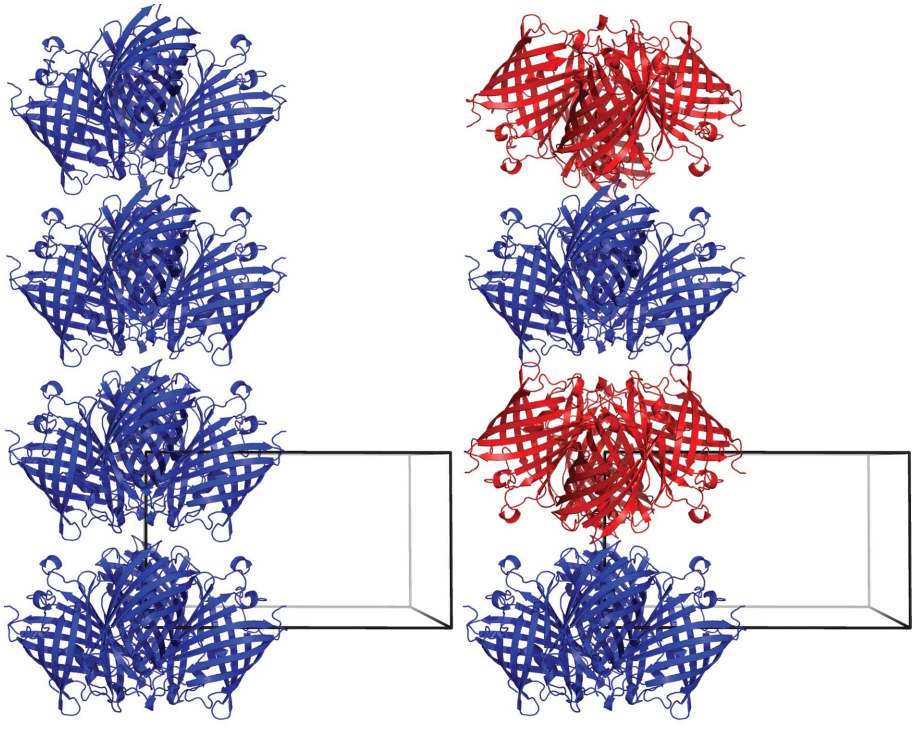

Figure 6
Possible associations of tetramers along the *z* crystal axis. (*a*) An example of a non-alternating stack consisting of similarly oriented tetramers. (*b*) An example of an alternating stack consisting of two groups of tetramers, blue and red, oriented 90° with respect to each other.

These stacks can associate laterally in numerous symmetrically different but energetically equivalent ways, providing irregular crystal growth. Fig. 7 shows four possible examples of such associations forming inclined linear and zigzag patterns within the diagonal plane of the unit cell and horizontal linear and chessboard patterns within the *xz* plane of the cell. The crystal contacts between stacks forming inclined linear (Fig. 7*a*) and zigzag (Fig. 7*b*) patterns are identical. In both cases, a central stack forms four (0° *x*, *y*, *z*–0° *x* + 1/2, *y* + 1/2, *z* + 1/2), two (90° *x*, *y*, *z*–90° *x* + 1/2, *y* + 1/2, *z* + 1/2) and four (0° *x*, *y*, *z*–90° *x* + 1/2, *y* + 1/2, *z* + 1/2) contacts with adjacent stacks. The contacts in the horizontal linear (Fig. 7*c*) and chessboard (Fig. 7*d*) patterns are not the same, but owing to the similar buried surface areas between similarly and alternatively oriented tetramers (67 and 52 Å^2, respectively) they are almost equivalent energetically. In a three-dimensional lattice, each stack is surrounded by eight neighbouring stacks and makes diagonal contacts with four of them and *x* and *y* contacts with four others. The diagonal contacts between stacks are realised through the octahedral faces of the cuboctahedron presented in Fig. 5 and the axial contacts are realised through its rhombic faces. Relative to each other, the neighboring stacks are shifted vertically, both up and down, by a half and a full cell repeat for the diagonally and axially associated stacks, respectively, producing energetically indistinguishable but symmetrically different patterns (Fig. 7). This enables a random distribution of alternatively oriented tetramers in the crystallographic array, resulting in the rotational OD crystal with statistically averaged *I*422 symmetry.

4. Conclusion

We have described the rotational order–disorder structure of the reversibly photoswitchable fluorescent protein rsTagRFP. It was demonstrated that the rotational OD crystal is formed by tetramers that are incorporated into the crystal array in two different orientations rotated by 90° with respect to each other. The occurrence of alternatively oriented tetramers in the crystal in partially correlated but otherwise stochastic arrangements causes degradation of the diffraction pattern, resulting in a statistically averaged *I*422 symmetry. The oversized contact areas

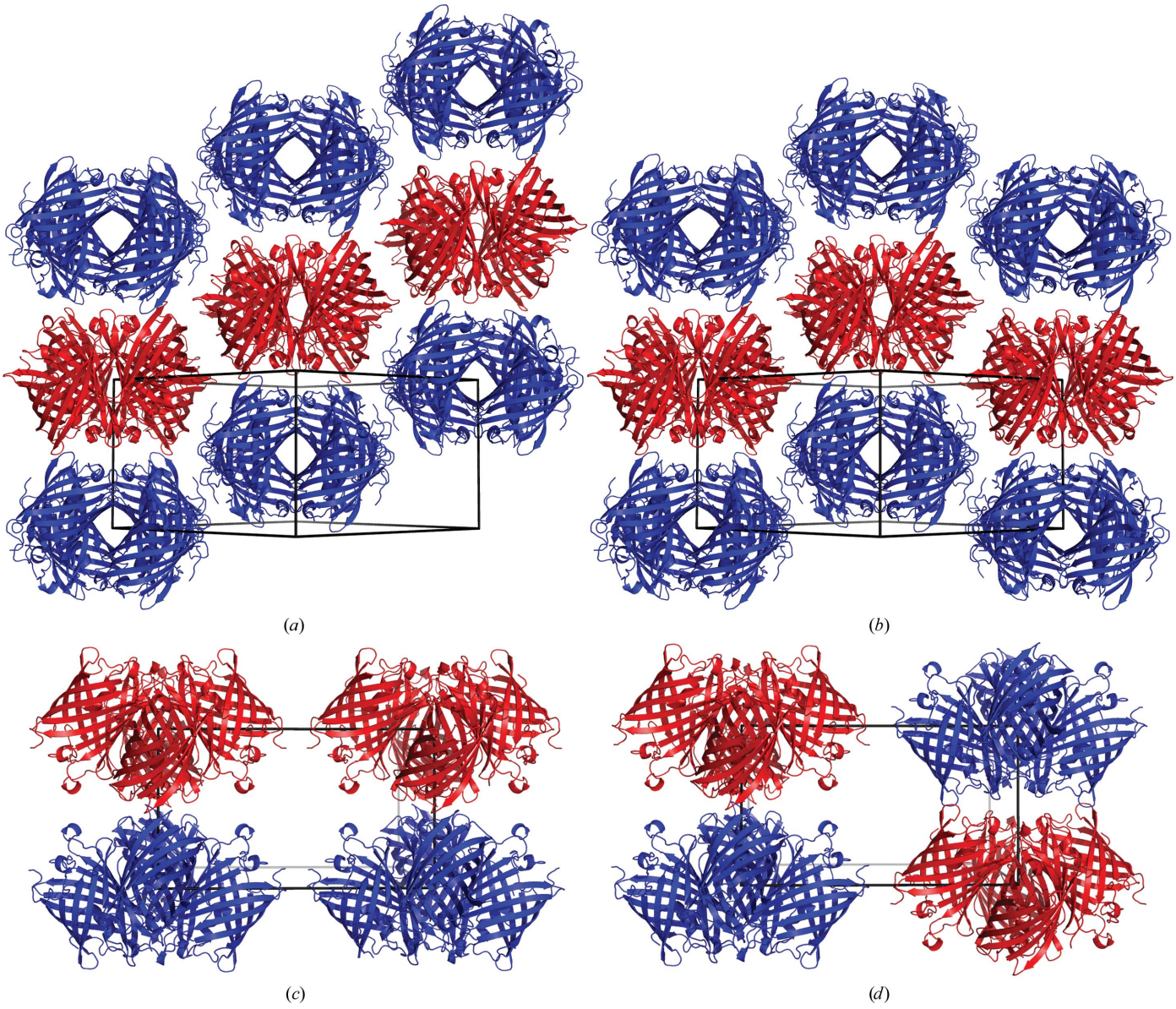

Figure 7
Examples of symmetrically different but energetically equivalent associations between stacks of alternatively oriented tetramers of rsTagRFP. (*a*) Tetramers forming an inclined linear pattern within the diagonal plane of the unit cell. (*b*) Tetramers forming a zigzag pattern within the diagonal plane. (*c*) Tetramers forming a horizontal linear pattern within the *xz* plane of the unit cell. (*d*) Tetramers forming a chessboard pattern within the *xz* plane.

between the tetramers along the *z* direction suggest that the tetramers can associate 'vertically', forming octamers or longer stacks in solution. Such unusual crystal packing is possible owing to the existence of several energetically equivalent but symmetrically different ways in which neighboring stacks can associate with each other.

Nowadays, powerful synchrotron sources, fast computers and contemporary software permit the investigation of difficult cases that were unsolvable mysteries two decades ago. The rotational OD crystal of rsTagRFP is an instructive example because the excellent quality electron density of rsTagRFP not only allows solution of the structure but also allows useful biological information to be obtained. This case demonstrates that pathological crystals should not be underestimated or neglected and that some difficult cases are worth revisiting, taking into account the advances in X-ray sources, computers and software.

Diffraction data were collected on the SER-CAT 22BM beamline at the Advanced Photon Source, Argonne National Laboratory. Use of the Advanced Photon Source was supported by the US Department of Energy, Office of Science, Office of Basic Energy Sciences under Contract No. W-31-109-Eng-38. This work was supported in part with Federal funds from the National Cancer Institute, National Institutes of Health (NIH) contract No. HHSN261200800001E, the Intramural Research Program of the NIH, the National Cancer Institute, the Center for Cancer Research and by NIH grants GM073913 and CA164468 to VVV. The content of this publication does not necessarily reflect the views or policies of

the Department of Health and Human Services, nor does the mention of trade names, commercial products or organizations imply endorsement by the US Government.

References

Adams, P. D. *et al.* (2010). *Acta Cryst.* D**66**, 213–221.
Birkedal, H., Bürgi, H.-B., Komatsu, K. & Schwarzenbach, D. (2003). *J. Mol. Struct.* **647**, 233–242.
Bonin, M., Welberry, T. R., Hostettler, M., Gardon, M., Birkedal, H., Chapuis, G., Möckli, P., Ogle, C. A. & Schenk, K. J. (2003). *Acta Cryst.* B**59**, 72–86.
Dauter, Z., Botos, I., LaRonde-LeBlanc, N. & Wlodawer, A. (2005). *Acta Cryst.* D**61**, 967–975.
Dhillon, A. K., Stanfield, R. L., Gorny, M. K., Williams, C., Zolla-Pazner, S. & Wilson, I. A. (2008). *Acta Cryst.* D**64**, 792–802.
Dornberger-Schiff, K. (1956). *Acta Cryst.* **9**, 593–601.
Dornberger-Schiff, K. (1966). *Acta Cryst.* **21**, 311–322.
Emsley, P. & Cowtan, K. (2004). *Acta Cryst.* D**60**, 2126–2132.
Ferraris, G., Makovicky, E. & Merlino, S. (2004). *Crystallography of Modular Matherials*. Oxford University Press.
Hwang, W. C., Lin, Y., Santelli, E., Sui, J., Jaroszewski, L., Stec, B., Farzan, M., Marasco, W. A. & Liddington, R. C. (2006). *J. Biol. Chem.* **281**, 34610–34616.
Janin, J. (1995). *Biochimie*, **77**, 497–505.
Janin, J., Bahadur, R. P. & Chakrabarti, P. (2008). *Q. Rev. Biophys.* **41**, 133–180.
Janin, J., Miller, S. & Chothia, C. (1988). *J. Mol. Biol.* **204**, 155–164.
Janin, J. & Rodier, F. (1995). *Proteins*, **23**, 580–587.
Laskowski, R. A., Rullmannn, J. A., MacArthur, M. W., Kaptein, R. & Thornton, J. M. (1996). *J. Biomol. NMR*, **8**, 477–486.
Lietzke, S. E., Carperos, V. E. & Kundrot, C. E. (1996). *Acta Cryst.* D**52**, 687–692.
Murshudov, G. N., Skubák, P., Lebedev, A. A., Pannu, N. S., Steiner, R. A., Nicholls, R. A., Winn, M. D., Long, F. & Vagin, A. A. (2011). *Acta Cryst.* D**67**, 355–367.
Otwinowski, Z. & Minor, W. (1997). *Methods Enzymol.* **276**, 307–326.
Padilla, J. E. & Yeates, T. O. (2003). *Acta Cryst.* D**59**, 1124–1130.
Pletnev, S., Morozova, K. S., Verkhusha, V. V. & Dauter, Z. (2009). *Acta Cryst.* D**65**, 906–912.
Pletnev, S., Subach, F. V., Dauter, Z., Wlodawer, A. & Verkhusha, V. V. (2012). *J. Mol. Biol.* **417**, 144–151.
Rye, C. A., Isupov, M. N., Lebedev, A. A. & Littlechild, J. A. (2007). *Acta Cryst.* D**63**, 926–930.
Schulze-Gahmen, U., Rini, J. M. & Wilson, I. A. (1993). *J. Mol. Biol.* **234**, 1098–1118.
Sheldrick, G. M. (2000). *XPREP* v.6.10. Bruker AXS, Madison, Wisconsin, USA.
Subach, F. V., Zhang, L., Gadella, T. W., Gurskaya, N. G., Lukyanov, K. A. & Verkhusha, V. V. (2010). *Chem. Biol.* **17**, 745–755.
Tanaka, S., Kerfeld, C. A., Sawaya, M. R., Cai, F., Heinhorst, S., Cannon, G. C. & Yeates, T. O. (2008). *Science*, **319**, 1083–1086.
Trame, C. B. & McKay, D. B. (2001). *Acta Cryst.* D**57**, 1079–1090.
Vagin, A. & Teplyakov, A. (2010). *Acta Cryst.* D**66**, 22–25.
Wang, J., Rho, S.-H., Park, H. H. & Eom, S. H. (2005). *Acta Cryst.* D**61**, 932–941.
Winn, M. D. *et al.* (2011). *Acta Cryst.* D**67**, 235–242.
Zhu, X., Xu, X. & Wilson, I. A. (2008). *Acta Cryst.* D**64**, 843–850.